The hyperfine structure in the rotational spectra of D2O: Lamb-dip measurements and quantum-chemical calculations

Gabriele Cazzoli, Luca Dore, Cristina Puzzarini, Jürgen Gauss

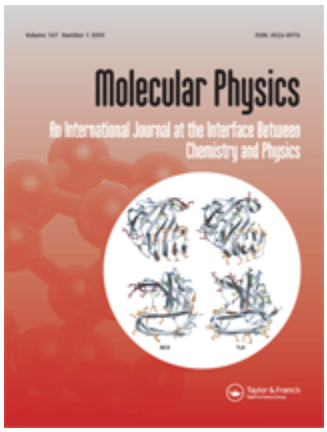

The hyperfine structure in the rotational spectra of D_2O: Lamb-dip measurements and quantum-chemical calculations

Journal:	*Molecular Physics*
Manuscript ID:	TMPH-2010-0032.R1
Manuscript Type:	Special Issue Paper -2 HRMS Stabia 09/ High Resolution Molecular Spectroscopy
Date Submitted by the Author:	30-Mar-2010
Complete List of Authors:	Cazzoli, Gabriele; Universita' di Bologna Dore, Luca; Universita' di Bologna Puzzarini, Cristina; Università di Bologna Gauss, Jürgen; Johannes-Gutenberg-Universität Mainz, Institut für Physikalische Chemie
Keywords:	D2O, rotational spectrum, hyperfine structure, Lamb-dip spectroscopy, quantum-chemical calculations
Note: The following files were submitted by the author for peer review, but cannot be converted to PDF. You must view these files (e.g. movies) online.	
D2O_ldip.tex	

The hyperfine structure in the rotational spectra of D_2O: Lamb-dip measurements and quantum-chemical calculations [1]

Gabriele Cazzoli, Luca Dore, Cristina Puzzarini *

Dipartimento di Chimica "G. Ciamician", Università di Bologna, Via Selmi 2, I-40126 Bologna, Italy

Jürgen Gauss

Institut für Physikalische Chemie, Universität Mainz, D-55099 Mainz, Germany

Abstract

Thirteen rotational transitions of the doubly deuterated isotopic species of water, $D_2{}^{16}O$, have been recorded in the millimeter- and submillimeter-wave region. The Lamb-dip technique has been used to resolve the hyperfine structure due to deuterium quadrupole coupling, due to spin-rotation as well as dipolar spin-spin interactions, thus enabling the determination of the corresponding hyperfine parameters to a good accuracy. The experimental investigation has been assisted by high-level quantum-chemical calculations of the hyperfine parameters.

Key words: D_2O, rotational spectrum, hyperfine structure, Lamb-dip spectroscopy, quantum-chemical calculations

1 Introduction

Water is a molecule of great importance in many areas of science. From a spectroscopic point of view, water vapor is an important constituent of the terrestrial atmosphere and plays a central role in the absorption of microwave

* corresponding author
Email address: cristina.puzzarini@unibo.it (Cristina Puzzarini).

[1] Special Issue: The 21th Colloquium on High Resolution Molecular Spectroscopy, Castellammare di Stabia August 31 - 4 September 2009

as well as infrared radiation of the atmosphere [1–3]. In addition, it is of astrophysical relevance as corresponding infrared and/or microwave transitions have been observed in sunspots [4], in the atmosphere of an extrasolar planet [5], and in the interstellar medium [6]. Although water and its isotopic species have been the subject of many experimental as well as theoretical investigations, its spectroscopic characterization is still incomplete. Strong centrifugal-distortion effects significantly affect the water spectra and hamper both the experimental determination of the spectroscopic parameters required to accurately reproduce all the observed transitions and to accurately predict those not measured [7–9] as well as the theoretical evaluation of rotational and vibrational frequencies [10].

Focusing in the following on the doubly deuterated species, $D_2{}^{16}O$, it should be noted that, although the rotational spectrum has been extensively investigated in selected frequency regions from 10 GHz up to 2.7 THz [9], to the best of our knowledge, no investigations have been reported with respect to its hyperfine structure in the millimeter- and submillimeter-wave ranges. For this reason, the Lamb-dip technique has been used in the present study to resolve the hyperfine structure of the rotational spectra as well as to provide transition frequencies with an accuracy of one order of magnitude, or even more, better than the standard techniques. The hyperfine structure of H_2O, HDO and D_2O has been investigated in the sixties by means of beam maser spectroscopy [11–14], but only incomplete information on the corresponding hyperfine parameters could be derived. Later on, in 1991, molecular beam electric resonance (MBER) measurements on the $J = 1_{1,1}$ and 1_{10} rotational states provided values for the diagonal elements of the deuterium quadrupole-coupling tensor as well as for various combinations of the diagonal deuterium spin-rotation constants [15].

The present paper is organized as follows. In the next section the experimental details are described. Thereafter, as the experimental investigation has been supported by quantum-chemical calculations, all computational details are provided. Finally, the results concerning the hyperfine parameters are reported and discussed.

2 Experiment

2.1 Spin statistics

According to Bose-Einstein statistics, the presence of two equivalent deuterium nuclei leads to the existence of *ortho* and *para* species. As the deuterium nuclear spin, I_D, is equal to 1, the total nuclear spin due to the coupling of

two deuterium spins, $I_{D,tot} = I_{D_1} + I_{D_2}$, can take the values 2, 1 and 0. The states with $I_{D,tot}$ equal to 2 or 0 correspond to *ortho*-D_2O, whereas the species with $I_{D,tot}$ equal to 1 is known as *para*-D_2O. Making use of the asymmetric-top notation, J_{K_a,K_c}, the *ortho* transitions are those for which the sum $K_a + K_c$ is even, whereas the *para* ones are those for which this sum is odd.

For both *para*- and *ortho*-D_2O, with the exception of the case $I_{D,tot} = 0$, the hyperfine structure (hfs) in the rotational spectrum is due to the interactions between the deuterium quadrupole moments Q and the electric-field gradients at the corresponding nuclei, interactions between the rotational angular momentum and the deuterium nuclear spin, and interactions between the nuclear spin momenta themselves. For both species, the various hyperfine components result from the ΔF=0,±1 selection rules, where F is the hyperfine quantum number due to the coupling scheme $F = J + I_{tot}$. To a generic $F' \leftarrow F$ transition corresponds only the $I_D = 1 \leftarrow 1$ transition in the case of *para*-D_2O, while the three cases $I_D = 2 \leftarrow 2$, $2 \leftarrow 0$ and $0 \leftarrow 0$ apply to the *ortho* species.

In the present study, seven *ortho* and six *para* rotational transitions have been recorded as described below. The former are $J = 6_{2,4} \leftarrow 7_{1,7}$, $5_{5,1} \leftarrow 6_{4,2}$, $5_{1,5} \leftarrow 4_{2,2}$, $7_{4,4} \leftarrow 6_{5,1}$, $5_{2,4} \leftarrow 4_{3,1}$, $7_{7,1} \leftarrow 8_{6,2}$, $2_{1,1} \leftarrow 2_{0,2}$, while the latter are $J = 6_{1,6} \leftarrow 5_{2,3}$, $4_{1,4} \leftarrow 3_{2,1}$, $5_{5,0} \leftarrow 6_{4,3}$, $1_{1,0} \leftarrow 1_{0,1}$, $7_{2,5} \leftarrow 8_{1,8}$, and $7_{7,0} \leftarrow 8_{6,3}$.

Figures 1 and 2 provide examples for the *ortho* and *para* transitions, thereby displaying the hyperfine structure of the $J = 2_{1,1} \leftarrow 2_{0,2}$ and $J = 1_{1,0} \leftarrow 1_{0,1}$ rotational transitions, respectively. They furthermore demonstrate the resolution that can be achieved by our experimental set up. In both figures the experimental spectra are furthermore compared to the calculated (frequency-modulated as well as stick) spectra, which will be commented on later in the text.

2.2 Experimental details

Lamb-dip measurements have been performed employing a frequency-modulated, computer-controlled spectrometer in conjunction with a conventional free-space cell, as shown in Ref. [16]. To increase the sensitivity of the spectrometer as well as the Lamb-dip effect, the radiation path has been doubled [17]. A detailed description of the spectrometer is given in Ref. [18], whereas our experimental set up for performing sub-Doppler resolution spectroscopy has been described in previous papers (see, for example, Refs. [19–21]). Therefore, we only report the main details that are of relevance for the present investigation. The millimeter- and submillimeter-wave sources employed are either frequency multipliers driven by Gunn-diode oscillators or Gunn diodes themselves, and the 90-400 GHz frequency range has been considered. The frequency modu-

lation is obtained by sine-wave modulating the 75 MHz local oscillator of the synchronization loop at 1.666 kHz. A liquid He-cooled InSb detector has been used, and its output has been processed by means of a Lock-in amplifier tuned at twice the modulation frequency. This leads, to a good approximation, to the recording of the second derivative of the natural line profile.

Measurements have been carried out at pressures of 0.5 mTorr, or even lower, employing a commercial sample of D_2O. Such low values of working pressure have been chosen to minimize the dip widths as much as possible in order to improve the resolution and in order to avoid pressure frequency shifts. In addition, the source power has been adequately reduced to have narrow and non-distorted dips. The modulation depth used has been adjusted in the 8-20 kHz range according to the experimental conditions and the transition under consideration. All measurements have been carried out at room temperature.

2.3 Analysis of the Spectra

As it is evident from Figures 1 and 2, a large number of lines are actually responsible for the observed features. We note that, in addition to the hyperfine (hf) components, crossing resonances, the so-called ghost transitions (also known as crossover resonances or simply crossovers), are present. This effect is due to the saturation of overlapping Gaussian profiles of two or more transitions with a common rotational energy level [22,23]. As already noted in previous investigations (see, for example, Refs. [19,20,24]), a line-profile analysis is necessary for correctly retrieving the hf component frequencies [16]; this implies that ghost transitions must be taken into account in such an analysis. Since a detailed description of the applied procedure has been given in Ref. [24], we only remind the reader that it is necessary to make a prediction of the spectrum containing only the hf components (real spectrum), of the spectrum containing only the crossover resonances (ghost spectrum), and of the spectrum containing both hf components and crossing resonances. This procedure allows to understand how the real spectrum is modified by the presence of ghost transitions and to take them properly into account in the line-profile analysis. We furthermore note that the accurate prediction of the intensity for the ghost transitions (see Ref. [25]) is essential for correctly reproducing the observed spectra. Figures 1 [2] and 2 provide representative examples, clearly demonstrating that ghost transitions cannot be neglected for a proper analysis. In fact, these figures show how the hfs changes when going from a situation in which only hf components are present to that in which both

[2] It should be noted that the small bump shown in Figure 1 at approximately 403562.1 MHz is due to poor baseline (accidentally resembling a very weak dip) and does not correspond to any spectral feature.

real and ghost transitions are considered. In both figures the stick spectra are also depicted, showing the hf components and the crossovers responsible for the actual spectrum recorded.

The line-profile analyses have been carried out iteratively by comparing in each step the graphical representation of the predicted spectra with the observed one. As starting point, the experimental values of nuclear quadrupole coupling constants from Ref. [15] and the theoretical predictions of spin-rotation and spin-spin interaction constants, computed as described in the following section, have been used. Already after the first step of the iterative analysis, almost all hf components and crossovers were properly assigned and the assignments were used to obtain a set of improved hyperfine parameters (by means of the fit described in the following). Based on these updated parameters, new predictions have been made and the procedure has been then repeated until a complete assignment of the recorded spectra and until close agreement between predicted and observed spectra.

The Hamiltonian used for fitting the retrieved frequencies is given as the following sum:

$$\mathbf{H} = \mathbf{H}_{ROT} + \mathbf{H}_{NQC} + \mathbf{H}_{SR} + \mathbf{H}_{SS} \ , \qquad (1)$$

where $\mathbf{H}_{ROT}$ is the usual rotational part of the Hamiltonian operator (see, for example, Ref. [26]), $\mathbf{H}_{NQC}$ is the nuclear quadrupole-coupling (NQC) Hamiltonian [26,27], $\mathbf{H}_{SR}$ is the Hamiltonian describing the spin-rotation (SR) interaction [27,28], and $\mathbf{H}_{SS}$ is the spin-spin (SS) Hamiltonian [27,28] accounting for the direct dipolar spin-spin interaction. While we do not go into detail with respect to $\mathbf{H}_{ROT}$, the other three Hamiltonians will be briefly addressed in the section describing our quantum-chemical calculations. The retrieved hf components as well as crossovers have been included in a least-squares fit in which each line frequency is weighted proportional to the inverse square of its experimental uncertainty. Ghost transitions have been considered as arithmetic mean of the frequencies of the two generating hf components. For blended features, the hf components and/or ghost transitions involved are weighted according to their intensities. The fit has been carried out with Pickett's SPCAT/SPFIT suite of programs [29] employing Watson's A-reduced Hamiltonian in the I^r representation [30].

The retrieved hf components as well as ghost-transition frequencies, obtained by the line-profile analyses and as averages of sets of measurements, are reported in the supplementary material (Table S1) together with the residuals (observed - calculated differences) from the fit described above. Experimental uncertainties are usually assigned based on the standard deviations of the averages of the measured values, but in the present case a more conservative estimate of the experimental uncertainties, i.e., 0.7 kHz, has been chosen. This estimate results to be conservative even when compared to the rms error of the measurement residuals, which is 0.63 kHz.

3 Computational details

All computations have been carried out using the CC singles and doubles (CCSD) approach augmented by a perturbative treatment of triple excitations (CCSD(T)) [31] with the basis-set convergence monitored by using the aug-cc-pCVnZ (n=T,Q,5,6) [32–36] hierarchical series of correlation-consistent basis sets. All electrons have been included in the electron-correlation treatment. The semi-experimental equilibrium structure (r(OH) = 0.9575 Å, ∠(HOH)= 104.51° [37]) has been used in the computations of the equilibrium values for the hyperfine parameters, while vibrational corrections have been computed at the optimized geometry corresponding to the level of theory considered. Second-order vibrational perturbation theory (VPT2) [38] has been used for evaluating the latter.

As the focus of the present investigation is on the determination of the nuclear quadrupole-coupling, spin-rotation, and spin-spin interaction constants, we will briefly summarize how these quantities are obtained by means of quantum-chemical calculations.

For the deuterium nuclei, which are the only ones with a nuclear quadrupole moment, the interaction of the latter with the electric-field gradient at the corresponding nuclei is responsible for the NQC (for details, see Refs. [26,27,39]). This is expressed by the following Hamiltonian:

$$\mathbf{H}_{NQC} = \frac{1}{2}\sum_K \frac{-eQ_K q_J^K}{I_K(2I_K-1)J(2J-1)}\left[3(\mathbf{I}_K\cdot\boldsymbol{J})^2+\frac{3}{2}(\mathbf{I}_K\cdot\boldsymbol{J})-\mathbf{I}_K^2\boldsymbol{J}^2\right], \tag{2}$$

where eQ_K and q_J^K denote the quadrupole moment and electric-field gradient of the K-th nucleus, respectively, and the sum runs over the two deuterium nuclei. The quantum-chemical computation of the NQC constants, denoted by χ, thus requires the determination of the corresponding electric-field gradients, which are first-order properties and accessible by means of analytic gradient techniques [40]. The required nuclear qudrupole-moment value of deuterium, 0.002860 mbarn, has been taken from Ref. [41].

The usual formulation for SR interaction is given in terms of a second-rank tensor $\mathbf{C}$ coupled with the rotational and nuclear spin momenta [42]:

$$\mathbf{H}_{SR} = \sum_K \mathbf{I}_K\cdot\mathbf{C}^K\cdot\boldsymbol{J}, \tag{3}$$

with the sum running over all K nuclei of the molecule having nonzero nuclear spin ($I \geq 1/2$, i.e., only the deuteriums in our case). Each element of the spin-rotation tensor has an electronic and a nuclear contribution. While the latter only depends on the molecular geometry, the electronic contribution is evaluated as second derivative of the electronic energy with respect to the rotational

angular momentum and the involved nuclear spin [28]. This is efficiently done using analytic second-derivative techniques [43–46]. Perturbation-dependent basis functions (often referred to as rotational London Atomic Orbitals [47]) have been employed to improve the basis-set convergence. It should be noted that we adopt a sign convention for spin-rotation constants opposite to that originally used by Flygare [42].

The dipolar interaction between two nuclear magnetic moments is described via the following Hamiltonian

$$\mathbf{H}_{SS}^{(KL)} = \mathbf{I}_K \cdot \mathbf{D}^{KL} \cdot \mathbf{I}_L \ , \tag{4}$$

with the expression for the components of the dipolar spin-spin coupling tensor $\mathbf{D}^{KL}$ given, for example, in Refs. [26,48,49]. It is seen that the dipolar-coupling tensor $\mathbf{D}^{KL}$ is completely determined once the molecular geometry is known, thus not requiring any knowledge of the electronic structure of the molecule. However, this strictly applies only to the case of a rigid, non-vibrating molecule, while experimentally derived values correspond to those averaged over the vibrational ground state of the molecule. Quantum-chemical calculations are needed to compute the zero-point vibrational (ZPV) corrections.

ZPV corrections to electric-field gradient, spin-rotation and spin-spin constants have been obtained using the perturbative approach described in Ref. [50] for NMR shielding tensors. This approach has already been employed in many cases to compute vibrational corrections for hyperfine parameters (see, for example, Refs. [51–57]). Going into details, the vibrational corrections are obtained by expanding the expectation value of the considered property over the vibrational wavefunction in a Taylor series around the equilibrium value with respect to normal-coordinate displacements and computing the required expectation values of the normal-coordinate displacements in a perturbative manner. Anharmonic effects, which contribute here in lowest order of perturbation theory, require the evaluation of the cubic force field. While the harmonic force field has been computed in a fully analytic manner [45], the cubic force field as well as the corresponding derivatives of the considered property have been obtained using finite-difference techniques as described in Refs. [43,58]. The vibrational corrections, defined as the difference between the vibrationally averaged and equilibrium values determined at the same computational level, have then been added to our best equilibrium results in order to derive theoretical best estimates for the ground-state data. The latter can be directly compared to the experimental values.

The CFOUR program package [59] has been employed for all quantum-chemical calculations reported in the present work.

4 Results and discussion

The experimental hf parameters obtained from the least-squares fit described above are gathered in Table 1, where they are also compared with the corresponding best theoretical estimates as well as with previous experimental determinations [13,15]. As the knowledge of the unperturbed frequencies for the rotational transitions investigated in the present work may turn out to be useful for different purposes, they have been derived and are reported in Table 2. They can be considered as the recommended unperturbed frequency values.

Both sets of previous experimental data reported in Table 1 deserves to be commented on. With respect to Ref. [15], it should be noted that all diagonal components of the nuclear quadrupole-coupling tensor have been determined, while for the spin-rotation interaction tensor only the sums C_{aa}+C_{bb} and C_{aa}+C_{cc} have been reported. For all of these parameters good agreement with our determinations is observed, i.e., the differences are lower than 1-2 times the given uncertainties. Concerning Ref. [13], we note that the diagonal components of the spin-rotation tensor were obtained by simultaneously analysing the data available for various isotopic species of water, namely, H_2O, HDO and D_2O, thereby making use of the rigid-rotor as well as some other approximations (for details see Refs. [13,42]). Though such a procedure led to good description of the experimental data [11,12], the authors themselves cast some doubts on their own analysis in a subsequent paper [14]. Nevertheless, we note a perfect agreement with our experimental as well as calculated values. As a sort of conclusion we point out that, even though our results are less accurate than those obtained from MBER and beam maser spectroscopies, the present study reports for D_2O the first, entirely experimental, determination of the diagonal deuterium spin-rotation tensor elements and of the direct spin-spin coupling constant. In Refs. [12–15] the latter was taken into consideration only as calculated value.

Concerning the comparison with our theoretical predictions, we note good agreement with discrepancies of less than 0.1 kHz for spin-rotation and spin-spin constants and less than 1 kHz for χ_{bb}-χ_{cc}, and of the order of 1 kHz for χ_{aa}. Therefore, the present investigation is a further confirmation of the fact that spectroscopic parameters can be accurately determined by quantum-chemical calculations [60]. In the following our theoretical results are discussed in some further details.

In Tables 3 and 4 complete lists of our computed values for the hyperfine parameters are given; in the former, the results concerning the nuclear quadrupole coupling are collected, while the latter reports those for spin-rotation and spin-spin interactions. The first conclusion that can be drawn is that in all

cases the convergence of the equilibrium values as well as of the vibrational corrections with increasing basis-set size is monotonic and smooth. Furthermore, in almost all cases (i.e., except the vibrational corrections to C_{ab} and D_{aa}) the absolute value decreases by enlarging the basis set. Going into further details, we note for the NQC constants that the equilibrium values can be considered converged at the CCSD(T)/aug-cc-pCVQZ level as the differences with the CCSD(T)/aug-cc-pCV6Z level are on average smaller than 1.5 kHz. These differences further reduce to less than 1 kHz when considering the CCSD(T)/aug-cc-pCV5Z level. In the present case, for which the NQC constants are quite small, the latter level of theory is at least required when aiming at quantitative predictions. As far as spin-rotation constants are concerned, the aug-cc-pCVQZ is already able to provide well converged results that differ from those obtained with the largest basis set only by about 1%, i.e., 0.01-0.04 kHz. In line with the results reported in Ref. [46], for D_2O correlation effects beyond CCSD(T) are small and can be safely ignored.

Concerning the vibrational corrections, as already outlined in Refs. [55,57], the VPT2 approach is suitable for their evaluation. Due to their small magnitude and due to the rather large basis-set demands, the larger aug-cc-pCVQZ basis is required in the case of the NQC constants to obtain converged values within 0.1 kHz, while due to the use of rotational London orbitals the use of the aug-cc-pCVTZ basis is sufficient in the case of the SR constants. In general, we note that for all hyperfine parameters the vibrational corrections are small though not negligible, as they range from 1% to 3%. Therefore, inclusion of vibrational corrections is mandatory for quantitative predictions.

5 Conclusion

Using the Lamb-dip technique, the hyperfine structures of thirteen rotational transitions of $D_2{}^{16}O$ have been resolved, and their analysis, guided by previous experimental data as well as quantum-chemical calculations, enabled for the first time the complete experimental determination of the corresponding hyperfine parameters. Good agreement with theoretical values obtained by means of high-level quantum-chemical calculations further demonstrates that computations can provide reliable reference values and therefore, if required, can support, guide or even replace experimental determinations.

6 Acknowledgments

This work has been supported by "PRIN 2007" funds (project "Trasferimenti di energia, carica e molecole in sistemi complessi") and by University

of Bologna (RFO funds) as well as in Mainz by the Deutsche Forschungsgemeinschaft and the Fonds der Chemischen Industrie.

Captions of the Tables

Table 1. Comparison of the experimental and calculated hyperfine parameters of $D_2{}^{16}O$.

Table 2. Unperturbed frequencies for the $J', K'_a, K'_c \leftarrow J, K_a, K_c$ rotational transitions (MHz) of $D_2{}^{16}O$ considered in this work.

Table 3. Basis-set convergence and vibrational corrections for the deuterium quadrupole-coupling constants of $D_2{}^{16}O$ (kHz). All reported calculations have been performed at the CCSD(T) level.

Table 4. Basis-set convergence and vibrational corrections for the spin-rotation and spin-spin constants of $D_2{}^{16}O$ (kHz). All reported calculations have been performed at the CCSD(T) level.

Captions of the Figures

Figure 1. The $J = 2_{1,1} \leftarrow 2_{0,2}$ rotational transition (*ortho*) of $D_2{}^{16}O$ recorded at P = 0.5 mTorr (mod. depth = 12 kHz). Calculated spectra for real hf components (in red), crossovers (in green) as well as both real and ghost transitions (in blue) are also depicted. Stick spectra of real and ghost transitions are also shown.

Figure 2. The $J = 1_{1,0} \leftarrow 1_{0,1}$ rotational transition (*para*) of $D_2{}^{16}O$ recorded at P = 0.5 mTorr (mod. depth = 6 kHz). Calculated spectra for real hf components (in red), crossovers (in green) as well as both real and ghost transitions (in blue) are also depicted. Stick spectra of real and ghost transitions are also shown.

References

[1] J. R. Pardo, E. Serabyn, and J. Cernicharo, *J. Quantit. Spectrosc. Radiat. Transfer* **68**, 419 (2001).

[2] J. R. Pardo, E. Serabyn, M. C. Wiedner, and J. Cernicharo, *J. Quantit. Spectrosc. Radiat. Transfer* **96**, 537 (2005).

[3] L. S. Rothman, I. E. Gordon, A. Barbe, D. Chris Benner, P. F. Bernath, M. Birk, V. Boudon, L. R. Brown, A. Campargue, J.-P. Champion, K. Chance, L. H. Coudert, V. Dana, V. M. Devi, S. Fally, J.-M. Flaud, R. R. Gamache, A. Goldman, D. Jacquemart, I. Kleiner, N. Lacome, W. J. Lafferty, J.-Y. Mandin, S. T. Massie, S. N. Mikhailenko, C. E. Miller, N. Moazzen-Ahmadi, O. V. Naumenko, A. V. Nikitin, J. Orphal, V. I. Perevalov, A. Perrin, A. Predoi-Cross, C. P. Rinsland, M. Rotger, M. Šimečková, M. A. H. Smith, K. Sung, S. A. Tashkun, J. Tennyson, R. A. Toth, A. C. Vandaele, J. Vander Auwera, *J. Quantit. Spectrosc. Radiat. Transfer* **110**, 533 (2009).

[4] O. L. Polyansky, N. F. Zobov, S. Viti, J. Tennyson, P. F. Bernath, and L. Wallace, *Science* **277**, 346 (1997).

[5] G. Tinetti, A. Vidal-Madjar, M.-C. Liang, J.-P. Beaulieu, Y. Yung, S. Carey, R. J. Barber, J. Tennyson, I. Ribas, N. Allard, G. E. Ballester, D. K. Sing, and F. Selsis, *Nature* (London) **448**, 169 (2007).

[6] H. M. Butner, S. B. Charnley, C. Ceccarelli, S. D. Rodgers, J. R. Pardo, B. Parise, J. Cernicharo, and G. R. Davis, *Astrophys J.* **659**, L137 (2007).

[7] P. Chen, J. C. Pearson, H. M. Pickett, S. Matsuura and G. A. Blake, *Astrophys. J. Suppl. Series* **128**, 371 (2000).

[8] H. M. Pickett, J. C. Pearson, and C. E. Miller, *J. Mol. Spectrosc.* **233**, 174 (2005).

[9] S. Brünken, H. S. P. Müller, C. Endres, F. Lewen, T. Giesen, B. Drouin, J. C. Pearson, and H. Mäder, *Phys. Chem. Chem. Phys.* **9**, 2103 (2007).

[10] O. L. Polyansky, A. G. Császár, S. V. Shirin, N. F. Zobov, P. Barletta, J. Tennyson, D. W. Schwenke, and P. J. Knowles, *Science* **299**, 539 (2003).

[11] H. Bluyssen, A. Dymanus, and J. Verhoeven, *Phys. Lett.* **24A**, 482 (1967).

[12] H. Bluyssen, J. Verhoeven, and A. Dymanus, *Phys. Lett.* **25A**, 214 (1967).

[13] H. Bluyssen, A. Dymanus, J. Reuss, and J. Verhoeven, *Phys. Lett.* **25A**, 584 (1967).

[14] J. Verhoeven, H. Bluyssen, and A. Dymanus, *Phys. Lett.* **26A**, 424 (1968).

[15] R. Bhattacharjee, J. S. Muenter, and M. D. Marshall, *J. Mol. Spectrosc.* **145**, 302 (1991).

[16] G. Cazzoli and L. Dore, *J. Mol. Spectrosc.* **143**, 231 (1990).

[17] L. Dore, C. Degli Esposti, A. Mazzavillani, and G. Cazzoli, *Chem. Phys. Lett.* **300**, 489 (1999).

[18] G. Cazzoli and L. Dore, *J. Mol. Spectrosc.* **141**, 49 (1990).

[19] G. Cazzoli, L. Dore, L. Cludi, C. Puzzarini, and S. Beninati, *J. Mol. Spectrosc.* **215**, 160 (2002).

[20] G. Cazzoli, L. Dore, C. Puzzarini, and S. Beninati, *Phys. Chem. Chem. Phys.* **4**, 3575 (2002).

[21] G. Cazzoli, C. Puzzarini, and A.V. Lapinov, *Astrophys. J.* **592**, L95 (2003).

[22] R. S. Winton, *Observations and Applications of the Lamb-dip in Millimeter-Wave Molecular Spectroscopy*, Ph.D. dissertation (Duke University, Durham, NC 1972).

[23] V. S. Letokhov and V. P. Chebotayev, *Nonlinear Laser Spectroscopy* (Springer-Verlag, Berlin/Heidelberg/New York, 1977) pp. 238-242, and references therein.

[24] G. Cazzoli and C. Puzzarini, *J. Mol. Spectrosc.* **233**, 289 (2005).

[25] G. Magerl, W. Schupita, J. M. Frye, W. A. Kreiner, and T. Oka, *J. Mol. Spectrosc.* **107**, 72 (1984).

[26] W. Gordy and R. L. Cook, *Microwave molecular spectra*, 3rd Edition, edited by A. Weissberger (Wiley, New York, 1984).

[27] C. H. Townes and A. L. Schawlow, *Microwave Spectroscopy* (McGraw-Hill, New York, 1955).

[28] W. H. Flygare, *Chem. Rev.* **74**, 653 (1974).

[29] H. M. Pickett, *J. Mol. Spectrosc.* **148**, 371 (1991).

[30] J. K. G. Watson, in *Vibrational Spectra and Structure*, Vol. 6, edited by J.R. Durig (Elsevier, New York/Amsterdam, 1977).

[31] K. Raghavachari, G. W. Trucks, J. A. Pople, and M. Head-Gordon, *Chem. Phys. Lett.* **157**, 479 (1989).

[32] T. H. Dunning, Jr., *J. Chem. Phys.* **90**, 1007 (1989).

[33] D. E. Woon and T. H. Dunning, Jr., *J. Chem. Phys.* **103**, 4572 (1995).

[34] A. K. Wilson, T. van Mourik, and T. H. Dunning, Jr., *J. Mol. Struct. (THEOCHEM)* **388**, 339 (1998).

[35] R. A. Kendall, T. H. Dunning, Jr., and R. J. Harrison, *J. Chem. Phys.* **96**, 6796 (1992).

[36] T. van Mourik, *Mol. Phys.* **96**, 529 (1999).

[37] K. L. Bak, J. Gauss, P. Jørgensen, J. Olsen, T. Helgaker, and J. F. Stanton, *J. Chem. Phys.* **114**, 6548 (2001).

[38] I. M. Mills, in *Molecular Spectroscopy: Modern Research*, edited by K. N. Rao and C. W. Mathews (Academic Press, New York, 1972).

[39] E. A. C. Lucken, *Nuclear Quadrupole Coupling Constants* (Academic Press, London/New York, 1969).

[40] J. D. Watts, J. Gauss, and R. J. Bartlett, *Chem. Phys. Lett.* **200**, 1 (1992).

[41] P. Pyykkö, *Z. Naturforsch.* **47A**, 189 (1991).

[42] W. H. Flygare, *J. Chem. Phys.* **41**, 793 (1964).

[43] J. F. Stanton and J. Gauss, *Int. Rev. Phys. Chem.* **19**, 61 (2000).

[44] J. Gauss and J. F. Stanton, *J. Chem. Phys.* **104**, 257 (1996).

[45] J. Gauss and J. F. Stanton, *Chem. Phys. Lett.* **276**, 70 (1997).

[46] M. Kállay and J. Gauss, *J. Chem. Phys.* **120**, 6841 (2004).

[47] J. Gauss, K. Ruud, and T. Helgaker, *J. Chem. Phys.* **105**, 2804 (1996).

[48] A. Abragam, *Principles of Nuclear Magnetism* (Oxford University Press, New York, 1961).

[49] K. Schmidt-Rohr and H.W. Spiess, *Multidimensional Solid State NMR and Polymers* (Academic Press, New York, 1994).

[50] A. A. Auer, J. Gauss, and J. F. Stanton, *J. Chem. Phys.* **118**, 10407 (2003).

[51] C. Puzzarini, S. Coriani, A. Rizzo, and J. Gauss, *Chem. Phys. Lett.* **409**, 118 (2005).

[52] A. Rizzo, C. Puzzarini, S. Coriani, and J. Gauss, *J. Chem. Phys.* **124**, 064302 (2005).

[53] G. Cazzoli, C. Puzzarini, S. Stopkowicz, and J. Gauss, *Mol. Phys.* **106**, 1181 (2008).

[54] H. Spahn, H. S. P. Müller, T. F. Giesen, J.-U. Grabow, M. E. Harding, J. Gauss, and S. Schlemmer, *Chem. Phys.* **346**, 132 (2008).

[55] G. Cazzoli, C. Puzzarini, M. E. Harding, and J. Gauss, *Chem. Phys. Lett.* **473**, 21 (2009).

[56] F. F. S. van der Tak, H. S. P. Müller, M. E. Harding, and J. Gauss, *Astron. & Astrophys.* **507**, 347 (2009).

[57] C. Puzzarini, G. Cazzoli, M. E. Harding, J. Vázquez, and J. Gauss, *J. Chem. Phys.* **131**, 234304 (2009).

[58] J. F. Stanton, C. L. Lopreore, and J. Gauss, *J. Chem. Phys.* **108**, 7190 (1998).

[59] CFOUR (Coupled Cluster techniques for Computational Chemistry), a quantum-chemical program package by J. F. Stanton, J. Gauss, M. E. Harding, and P. G. Szalay with contributions from A. A. Auer, R. J. Bartlett, U. Benedikt, C. Berger, D. E. Bernholdt, Y. J. Bomble, O. Christiansen, M. Heckert, O. Heun, C. Huber, T.-C. Jagau, D. Jonsson, J. Jusélius, K. Klein, W. J. Lauderdale, D. Matthews, T. Metzroth, D. P. O'Neill, D. R. Price, E. Prochnow, K. Ruud, F. Schiffmann, S. Stopkowicz, M. E. Varner, J. Vázquez, J. D. Watts, F. Wang and the integral packages MOLECULE (J. Almlöf and P. R. Taylor), PROPS (P. R. Taylor), ABACUS (T. Helgaker, H. J. Aa. Jensen, P. Jørgensen, and J. Olsen), and ECP routines by A. V. Mitin and C. van Wüllen. For the current version, see http://www.cfour.de

[60] C. Puzzarini, J. F. Stanton, and J. Gauss, *Int. Rev. Phys. Chem.*, accepted for publication (2010).

Table 1
Comparison of the experimental and calculated hyperfine parameters of $D_2{}^{16}O$.

Parameter		This work		MBER[a]	MASER[b]
		Experiment	Theory[c]	(1991)	(1968)
χ_{aa}(D)	(kHz)	152.55(88)	153.7	153.92(11)	
χ_{aa}^{K}(D)[d]	(kHz)	-0.289(59)			
(χ_{bb}-χ_{cc})(D)	(kHz)	198.03(76)	198.6	197.16(11)	
C_{aa}(D)	(kHz)	-2.89(26)	-2.98		-2.99(1)
C_{bb}(D)	(kHz)	-2.43(18)	-2.41		-2.36(2)
C_{aa}(D)+C_{bb}(D)	(kHz)	-5.32(31)[e]	-5.38	-5.353(11)	-5.35(2)[e]
C_{cc}(D)	(kHz)	-2.62(15)	-2.62		-2.64(1)
C_{aa}(D)+C_{cc}(D)	(kHz)	-5.51(30)[e]	-5.60	-5.56(11)	-5.63(1)[e]
D_{aa}(D-D)	(kHz)	-1.57(41)	-1.61		
σ[f]	(kHz)	0.63			
$\overline{\chi^2}$ [g]		0.89			

[a] Ref. [15].

[b] Ref. [13].

[c] Equilibrium value obtained at the CCSD(T)/aug-cc-pCV6Z level augmented by vibrational corrections obtained at the CCSD(T)/aug-cc-pCV5Z level.

[d] Dependence on K of χ_{aa}.

[e] Derived values.

[f] RMS error.

[g] Dimensionless (weighted) standard deviation.

Table 2
Unperturbed frequencies for the $J', K'_a, K'_c \leftarrow J, K_a, K_c$ rotational transitions (MHz) of $D_2{}^{16}O$ considered in this work.

Transition						Freq.
J'	K'_a	K'_c	J	K_a	K_c	(MHz)
6	1	6	5	2	3	93350.1855(9)
6	2	4	7	1	7	104875.7306(13)
4	1	4	3	2	1	151710.3774(7)
5	5	1	6	4	2	180171.1477(14)
5	1	5	4	2	2	181833.1754(10)
5	5	0	6	4	3	187633.2526(12)
7	4	4	6	5	1	192519.5039(15)
1	1	0	1	0	1	316799.8414(4)
5	2	4	4	3	1	339035.1096(10)
7	2	5	8	1	8	393332.8076(13)
7	7	1	8	6	2	403251.6307(20)
7	7	0	8	6	3	403377.3415(17)
2	1	1	2	0	2	403561.9929(7)

Table 3
Basis-set convergence and vibrational corrections for the deuterium quadrupole-coupling constants of $D_2{}^{16}O$ (kHz). All reported calculations have been performed at the CCSD(T) level.

Basis set	χ_{aa}	χ_{bb}	χ_{cc}	χ_{ab}=χ_{ba}
Equilibrium values[a]				
aug-cc-pCVTZ	166.277	23.183	-189.460	±233.303
aug-cc-pCVQZ	157.806	22.539	-180.345	±220.110
aug-cc-pCV5Z	156.813	22.489	-179.302	±218.505
aug-cc-pCV6Z	156.373	22.456	-178.829	±217.798
Vibrational corrections				
aug-cc-pCVTZ	-3.262	+0.095	+3.166	∓4.785
aug-cc-pCVQZ	-2.711	+0.003	+2.707	∓4.041
aug-cc-pCV5Z	-2.689	-0.004	+2.693	∓4.006

[a] Computed at the semi-experimental geometry: r(OH) = 0.9575 Å, ∠HOH = 104.51 degrees [37].

Table 4
Basis-set convergence and vibrational corrections for the spin-rotation and spin-spin constants of $D_2{}^{16}O$ (kHz). All reported calculations have been performed at the CCSD(T) level.

Basis set	C_{aa}	C_{bb}	C_{cc}	C_{ab}	C_{ba}	D_{aa}
Equilibrium values[a]						
aug-cc-pCVTZ	-3.156	-2.533	-2.802	±1.683	±4.266	
aug-cc-pCVQZ	-3.078	-2.468	-2.737	±1.633	±4.153	
aug-cc-pCV5Z	-3.057	-2.448	-2.718	±1.619	±4.122	
aug-cc-pCV6Z	-3.048	-2.441	-2.710	±1.614	±4.110	-1.630[b]
Vibrational corrections						
aug-cc-pCVTZ	+0.073	+0.036	+0.090	±0.008	±0.069	+0.016
aug-cc-pCVQZ	+0.073	+0.036	+0.089	±0.007	±0.071	+0.017
aug-cc-pCV5Z	+0.073	+0.035	+0.089	±0.007	±0.071	+0.017

[a] Computed at the semi-experimental geometry: $r(\mathrm{OH}) = 0.9575$ Å, $\angle\mathrm{HOH} = 104.51$ degrees [37].

[b] D_{aa} equilibrium values depend only on molecular structure (see text).

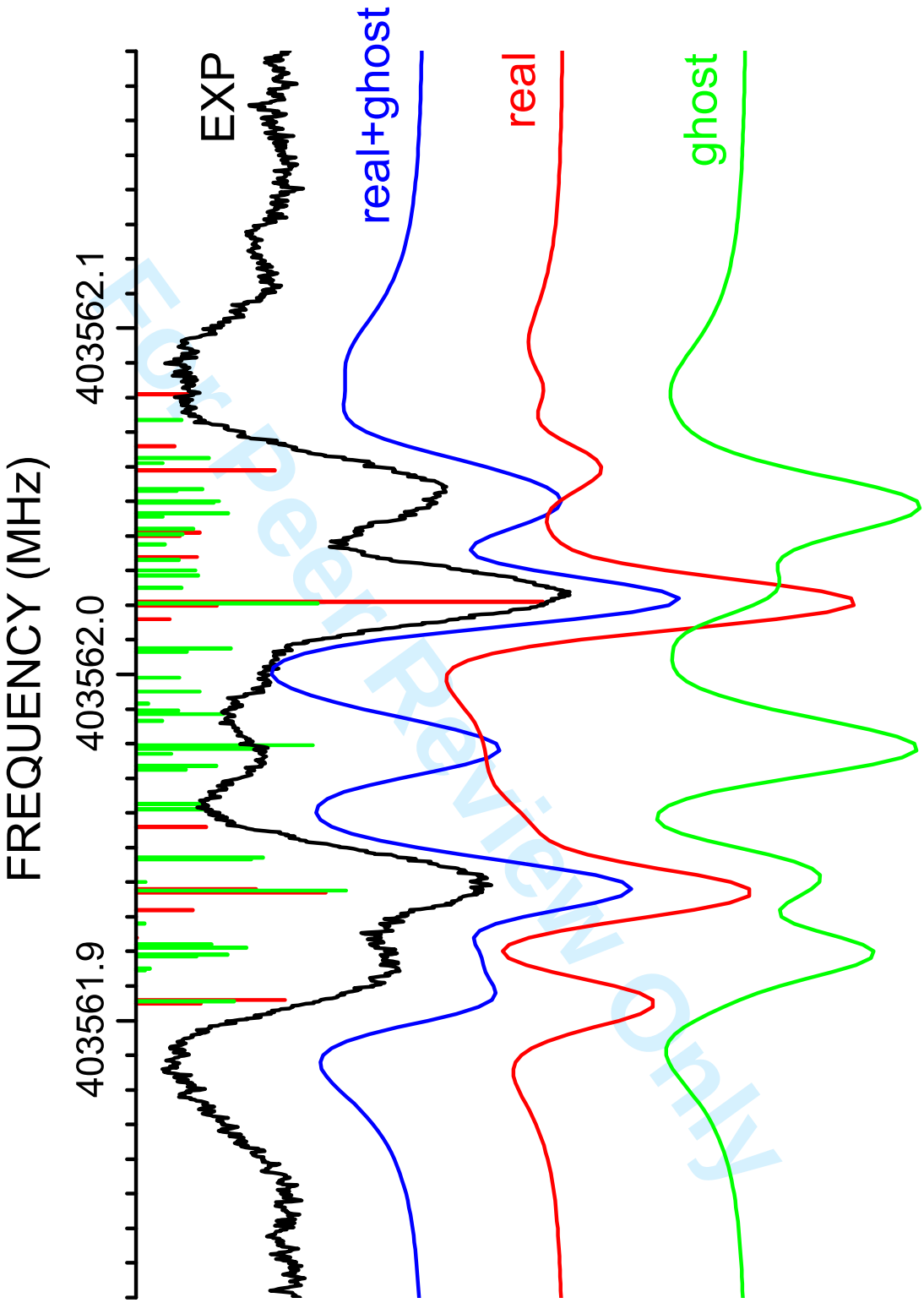

Fig. 1. The $J = 2_{1,1} \leftarrow 2_{0,2}$ transition of $D_2^{16}O$.

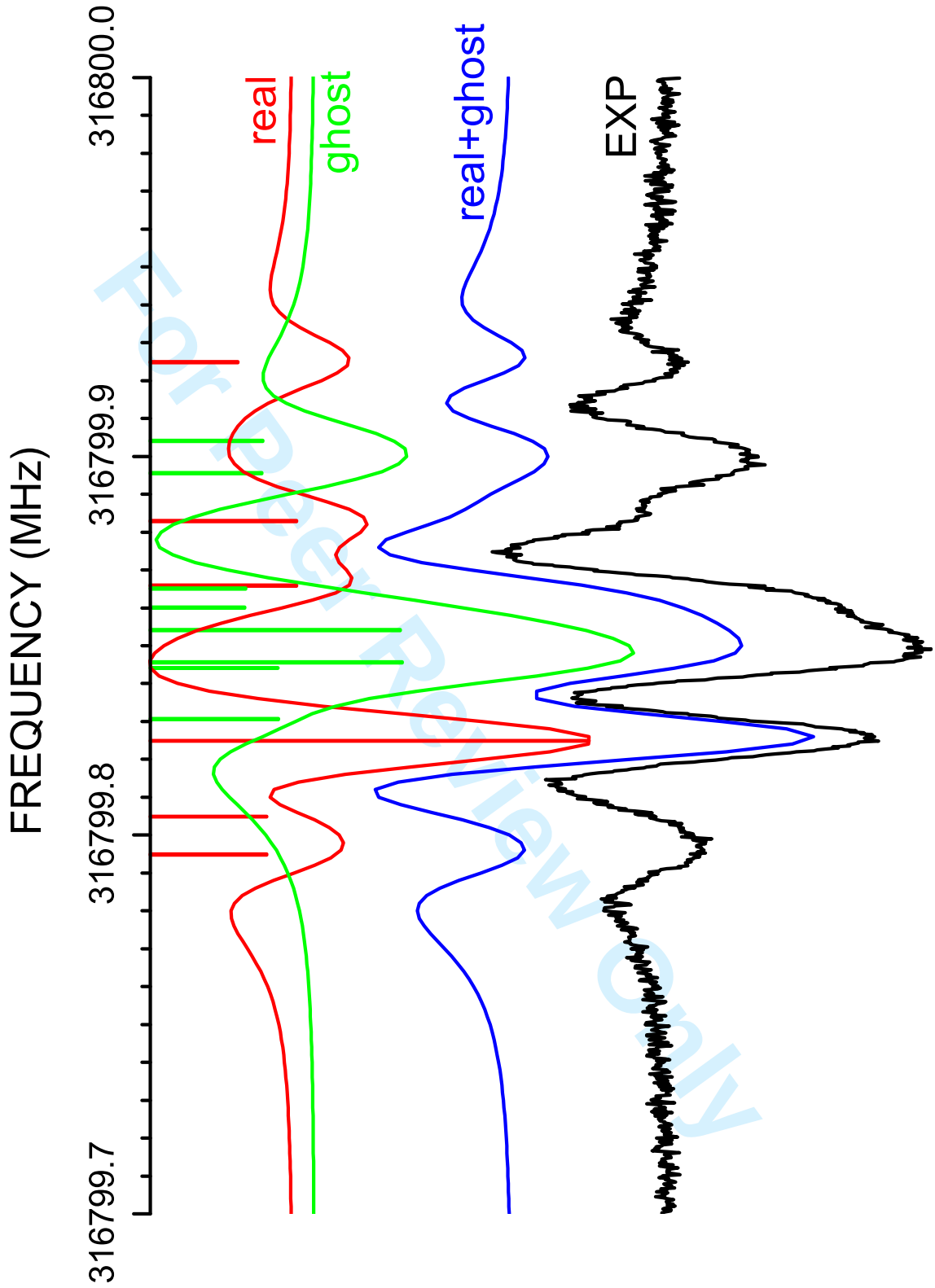

Fig. 2. The $J = 1_{1,0} \leftarrow 1_{0,1}$ transition of $D_2^{16}O$.

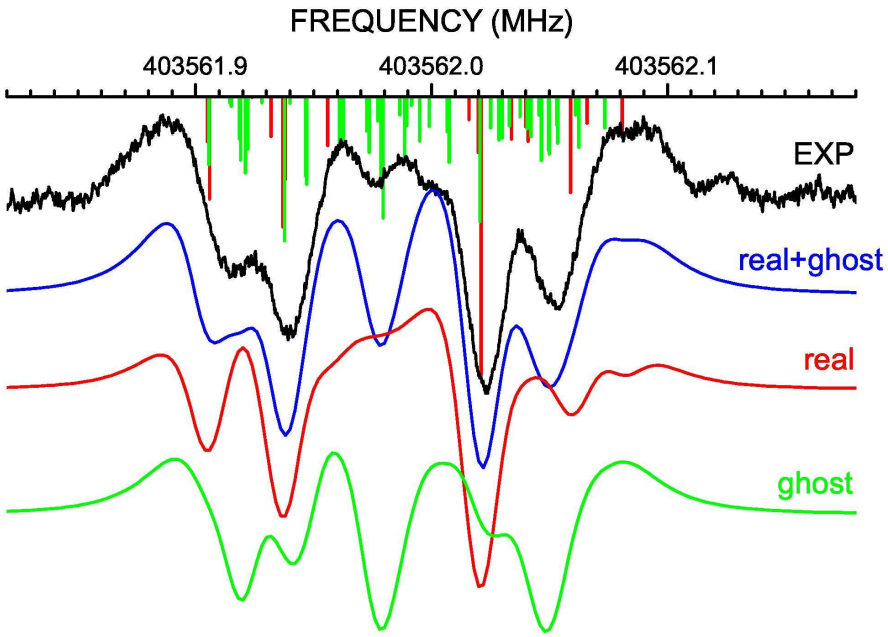

The J = $2_{1,1} \leftarrow 2_{0,2}$ rotational transition (ortho) of $D_2{}^{16}O$ recorded at P = 0.5 mTorr (mod. depth = 12 kHz). Calculated spectra for real hf components (in red), crossovers (in green) as well as both real and ghost transitions (in blue) are also depicted. Stick spectra of real and ghost transitions are also shown.
92x71mm (600 x 600 DPI)

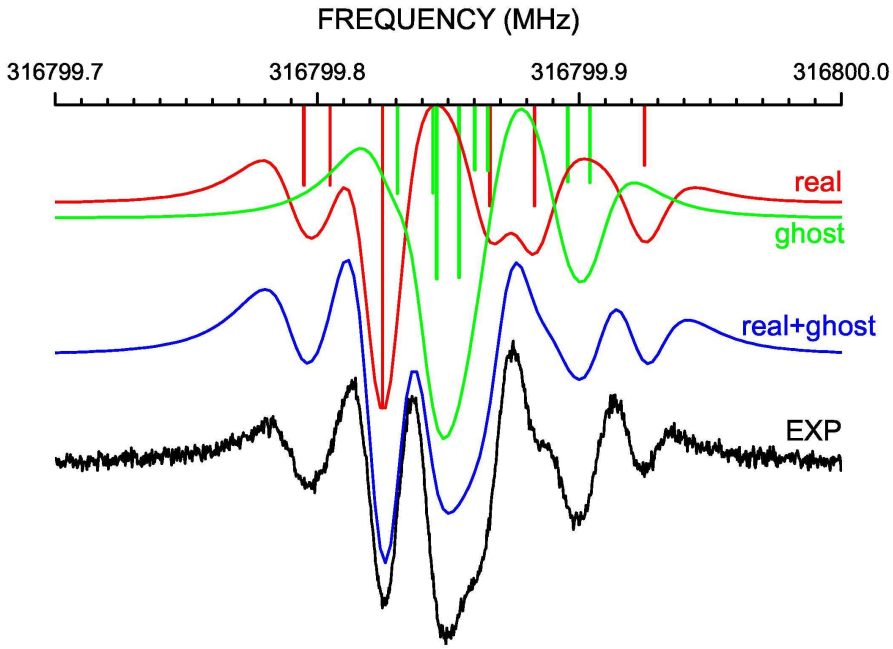

The J = $1_{1,0} \leftarrow 1_{0,1}$ rotational transition (ortho) of $D_2{}^{16}O$ recorded at P = 0.5 mTorr (mod. depth = 6 kHz). Calculated spectra for real hf components (in red), crossovers (in green) as well as both real and ghost transitions (in blue) are also depicted. Stick spectra of real and ghost transitions are also shown.
100x75mm (600 x 600 DPI)